
Proceedings Paper:
Poluri, N., De Souza, M.M. orcid.org/0000-0002-7804-7154, Venkatesan, N. et al. (1 more author) (2021) Modelling challenges for enabling high performance amplifiers in 5G/6G applications. In: 2021 28th International Conference on Mixed Design of Integrated Circuits and System. 28th International Conference on Mixed Design of Integrated Circuits and System (MIXDES), 24-26 Jun 2021, Lodz, Poland (online). IEEE (Institute of Electrical and Electronics Engineers) , pp. 45-50. ISBN 9781665443487

https://doi.org/10.23919/MIXDES52406.2021.9497644

Modelling Challenges for Enabling High Performance Amplifiers in 5G/6G applications

Nagaditya Poluri, Maria Merlyne DeSouza
Electrical and Electronics Engineering
The University of Sheffield, Sheffield, UK
m.desouza@sheffield.ac.uk

Nivedhita Venkatesan, Patrick Fay
Dept. of Electrical Engineering
University of Notre Dame, Notre Dame, IN USA

***Abstract*— Continuum mode amplifiers, which rely on harmonic tuning, have shown their potential for high efficiency over large bandwidths below 6 GHz and are strong candidates for even higher frequency applications of 5G networks. An accurate model of the transistor up to the third harmonic is a necessity for exploiting these amplifier classes. In this work, we present the considerations and challenges associated with modelling the device, and in particular the impact of extrinsic parasitics, for operation at high frequencies. We present a modified version of Dambrine's extraction procedure of intrinsic elements at sub-6 GHz frequencies, and demonstrate its utility up to 80 GHz by application in the extraction of a simulated GaN HEMT .**

***Keywords*—Fifth Generation mobile communication (5G), GaN HEMT, Parasitc extraction, Device modelling.**

I. INTRODUCTION

High efficiency broadband power amplifiers (PA) are critical for the realization of fifth-generation (and beyond) mobile communications networks. Accurate modelling of the transistor in the PA is one the main challenges to high performance. In the frequency range from 20-50 GHz, GaN HEMTs have demonstrated efficiency comparable to or better than Silicon CMOS, SiGe HBT, GaAs pHEMT, but at a higher output power [1]. This can be attributed to the high-breakdown voltage capability of GaN that can be exploited in continuum mode amplifiers. Continuum-mode designs reach a peak drain voltage 3 times the quiescent drain bias (V_{dsq}), rather than 2 times V_{dsq} in conventional class B, to achieve high efficiency over broad bandwidth. Class B/J/J*[2], CCF^{-1}[3][4], and class BJF^{-1} [5] are some examples of continuum modes that require tuning up to at least the second harmonic. Other continuous modes, such as CCF and class BJF, require tuning up to the third harmonic highlighting the need for accurate modelling upto this frequency of operation. Apart from increased costs of microwave instrumentation and uncertainty during measurement at higher frequency and power, the scaling properties of the model of a unit-cell device, to that of an actual multicell counterpart, presents an additional challenge, as the wavelength of the signal becomes comparable to the size of the device [6]. The suitability of a model is another important consideration.

In the initial phase of development, physical and quasi-physical models of the transistor, which rely on the properties of the material and physical effects at its interfaces, are essential to predict and optimize the structure for specific applications. COMON (the Compact Modeling Network) model, MIT Virtual Source GaNFET high-voltage (MVSG-HV) model and the HSP (HEMT Surface-Potential) model are some popularly used semi-physical models [7]. Although demonstrated to have the potential for accuracy, these models are still computationally intensive and time-consuming.

Table-based models represent another extreme in which the measured data of the device is used to fit predefined numerical functions, which may or may not have any physical significance. This approach, being entirely empirical, is able to accurately reflect the performance of devices, and is faster in simulations. X-parameters, which are an extension of S-parameters to include device non-linearity at high power, offer one such example [8]. However, models of this type can only be used within the range of inputs for which the measurement data is available, the fitting functions need to be differentiable up to high orders to be convergent in the simulator. Attempting to use the model beyond the measured data range can result in unexpected, non-physical, outcomes. Characterization of the device may not be possible for the entire desired range of inputs due to stability issues and limitations of the measurement setup.

Empirical models (i.e., equivalent circuit based models) offer a compromise in terms of simplicity, ease of implementation, accuracy and usefulness for circuit design [9]. In this case, the physical phenomenon is modelled by a lumped-element equivalent, or by empirical, or table-based models. For instance, thermal effects are often modelled by an RC circuit, while the I-V characteristics of the device may be empirical or table-based. Extraction of parameters of the model parameters based on pulsed I-V and continuous-wave (CW) S-parameters is often the initial step in the modelling process. Empirical models such as CFET, EEHEMT, Angelov [10], Angelov GaN [11], and Auriga are proposed for modelling HEMTs which have approximately 48, 71, 80, 90, and 100 model parameters [12]. These models are often further optimized to fit load-pull measured data which may compromise DC IV and/or S-parameter fitting [7]. DynaFET (Dynamic FET) [13] represents a further evolution wherein waveform information is simultaneously extracted as well as based on non-linear vector network analyzer (NVNA) measurements.

In this work, we present an empirical model, which is a simplified version of the Angelov model and has been used successfully in amplifier design below 6 GHz [14]. The extraction procedure used is a modified version of those proposed by Dambrine [15], Flores [16], and Lin [17]. We present the challenges and consideration of the extrinsic

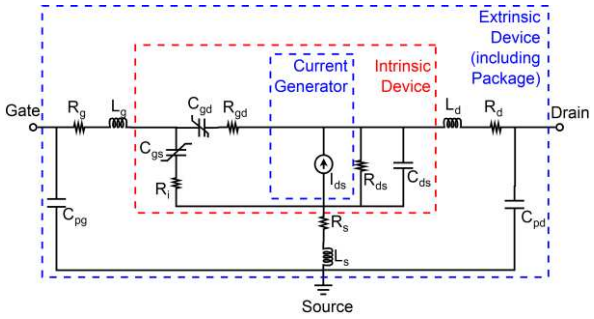

Fig. 1. The equivalent circuit of a GaN HEMT up to 6 GHz.

parasitics at high frequencies. The extraction of intrinsic parasitics in this procedure, which is proposed and validated for sub-6 GHz frequencies [18], is validated for a 50 nm x 75 µm GaN HEMT for frequencies up to 80 GHz. Owing to the simplicity of the extraction procedure, it can be easily applied even at very high frequencies.

II. EQUIVALENT CIRCUIT MODEL OF DEVICE

Parasitic effects arise within the structure of the device. An equivalent circuit of a transistor, considering parasitic effects is shown in Fig. 1 [15], [19]–[21]. Of these, the drain-pad capacitance (C_{pd}), gate-pad capacitance (C_{pg}), resistances (drain (R_d), source (R_s), and gate (R_g) resistances) and inductances (source (L_s), gate (L_g), and drain (L_d) inductances) are bias independent, whereas the intrinsic capacitance (drain-source capacitance (C_{ds}), gate-source (C_{gs}), and gate-drain capacitance (C_{gd})), output conductance (g_{ds}), R_i, and R_{ds} are bias dependent. While this type of model has been shown to be capable of accurately modelling the S-parameters of GaAs pHEMTs up to 40 GHz [19], for packaged GaN HEMTs the frequency limits are typically lower, at around 6 GHz [20]. Accuracy can be improved by adding additional extrinsic elements to more accurately model the parasitic effects in the device, with 20-element [22] or 22-element [23] models shown to be accurate up to 20 GHz. The small-signal equivalent model of a transistor may be extracted from its S-parameters at the bias point by optimizing the component values until the s-parameters of the model matches with measurement [24]. The optimal values of the component obtained by this approach depend on the optimization method, error function and the initial values [15]. An extraction process can be used to obtain approximate values of the elements of the model [15] from measurement which are then utilized as initial guess for optimization of the model.

A. *Extraction of extrinsic parameters*

Extrinsic parasitic elements can be extracted from the S-parameters of the device at cold condition (V_{ds}=0 V). The extrinsic pad capacitances are extracted from *cold pinch-off condition* ($V_{gs} < V_{th}$ and V_{ds} = 0 V) [15][16]. At this bias, the equivalent circuit of a device is simplified, as the intrinsic device can be represented by a π network of three capacitors (C_{gs}, C_{gd}, and C_{ds}) [15][16]. On the other hand, extrinsic resistances and inductances can be extracted from *cold forward condition* ($V_{gs}>V_{th}$ and V_{ds}=0). The accurate modelling of the extrinsic device, such as pads and connecting lines, is critical for high frequency device modelling, requiring additional elements in the equivalent circuit in Fig. 1.

As the number of elements increases, the number of equations required to solve for all unknowns also increases. The number of measurements can be increased to extract these additional elements. The model of the package can be extracted from 3-D electromagnetic (EM) simulations if its dimensions and layout are available [25]. This aspect can be important, especially for evaluating the power distribution in the feed structure as well as thermal analysis. Another approach is to attempt to establish relationships between the extrinsic and/or intrinsic capacitances [22]. These relationships can be based on the device structure or based on theoretical modelling of the device. However, this approach is challenging when details of the device layout are unavailable [26]. As an example, in [16], the ratio between the extrinsic capacitances are obtained by optimization of the difference between modelled and measured S-parameters. Such techniques may not be suitable at the frequencies for 5G applications.

An alternative method to increase the accuracy of the model is to represent the extrinsic parasitic effects originating from the metal lines at the gate, drain and source terminals and the package by transmission lines, rather than as lumped components. This approach enables the spatial distribution of the device to be naturally incorporated into the model. The transmission line is able to model the phase variation along the fingers of a transistor, as illustrated in Fig. 2 (a). Hence, such models can accurately model transistors at frequencies higher than 100 GHz. An example of a distributed model is shown in Fig. 2 (b). Here, the transistor is modelled as an interconnect of

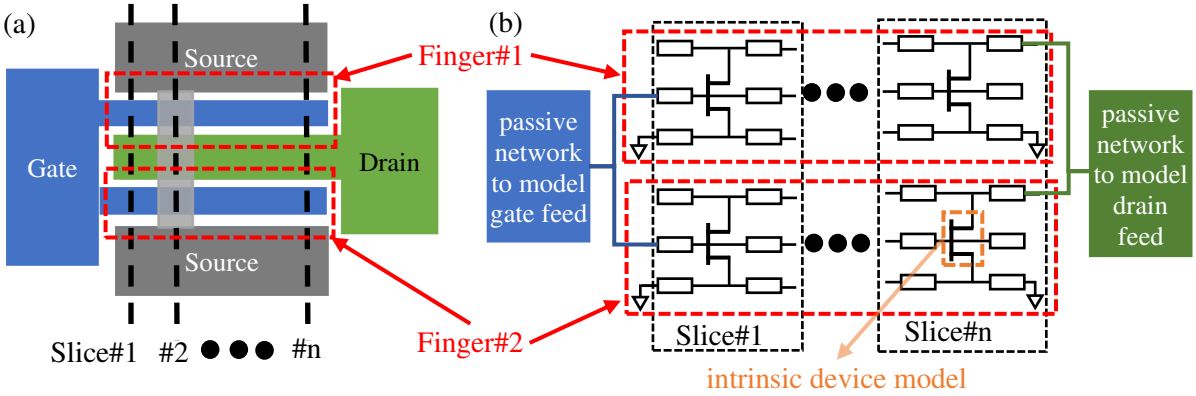

Fig. 2. (a) Top view of a simplified layout of a GaN HEMT transistor (b) High frequency distributed model of the transistor [6]

n slices (cross-section) of a transistor. Each finger in a slice is modelled by the intrinsic model of the transistor with parasitic elements, similar to the intrinsic device highlighted in Fig. 1. These intrinsic models for the gate, source, and drain terminals of the intrinsic device are connected by transmission lines whose lengths and widths are dependent on the number of slices and the widths of the gate, source and drain terminals respectively. If the slices are sufficiently small, these transmission lines can also be modelled by lumped passive elements [6]. The gate and drain terminals of the device to which the fingers connect are modelled by passive networks. Such an approach has been shown capable of modelling a device up to 150 GHz [6] by using 8 slices. Similarly, the transistor is modelled in [27] as an interconnect of 3 sections; one section is a cross-section with an air bridge (slice#2 in Fig. 2 (a)) with the other two sections on either side of the air bridge. This model was able to model a GaN HEMT up to 300 GHz. It is evident that the extraction of the extrinsic parasitic elements is critical for realizing accurate models of PAs for 5G and beyond.

B. *Extraction of Intrinsic parameters*

The non-linear intrinsic capacitances are extracted from S-parameters of the device at multiple bias points. For each bias point, the extrinsic elements are de-embedded from it's S-parameters, as illustrated by Dambrine in [15]. The equivalent circuit of the device after de-embedding elements is shown in Fig. 3.

1) Curve Fitting based methods

The Y parameters of the intrinsic device in Fig. 3 (Y^i) can be expressed as [15]

$$Y_{11}^i = R_i C_{gs}^2 \omega^2 / D + j\omega\left(C_{gs}/D + C_{gd}\right) \quad (1)$$

$$Y_{21}^i = g_m \exp(-j\omega\tau)/\left(1 + jR_i C_{gs}\omega\right) - j\omega C_{gd} \quad (2)$$

$$Y_{12}^i = -j\omega C_{gd} \quad (3)$$

$$Y_{22}^i = g_{ds} + j\omega\left(C_{ds} + C_{gd}\right) \quad (4)$$

Where $D = 1 + \omega^2 C_{gs}^2 R_i^2$. Since $\omega^2 C_{gs}^2 R_i^2 \approx 0$ for low frequencies [16][15], the admittance (Y_{gs}, Y_{gd}, Y_{gm}, and Y_{ds}) of the branches of the equivalent circuit can be approximated as

$$Y_{gs} = Y_{11}^i + Y_{12}^i \approx R_i C_{gs}^2 \omega^2 + j\omega C_{gs} \quad (5)$$

$$Y_{gd} = -Y_{12}^i = j\omega C_{gd} \quad (6)$$

$$Y_{gm} = Y_{21}^i - Y_{12}^i = g_m \exp(-j\omega\tau) \Big/ 1 + jR_i C_{gs}\omega \quad (7)$$

$$Y_{ds} = Y_{22}^i + Y_{12}^i = g_{ds} + j\omega C_{ds} \quad (8)$$

The individual elements from equations were separated as [16][22]

$$\omega C_{gd} = Im\left(Y_{gd}\right) = -Im\left(Y_{12}^i\right) \quad (9)$$

$$\omega R_i = \left(Re(Y_{11}) + Re(Y_{12})\right)/C_{gs}\left(Im(Y_{11}) + Im(Y_{12})\right) \quad (10)$$

$$\omega C_{ds} = Im(Y_{ds}) = Im(Y_{22}) + Im(Y_{12}) \quad (11)$$

$$g_{ds} = Re(Y_{ds}) = Re(Y_{22}) + Re(Y_{12}) \quad (12)$$

$$\omega C_{gs} \approx \left(Im(Y_{11}) + Im(Y_{12})\right)\left(1 + \frac{\left(Re(Y_{11}) + Re(Y_{12})\right)^2}{\left(Im(Y_{11}) + Im(Y_{12})\right)^2}\right) \quad (13)$$

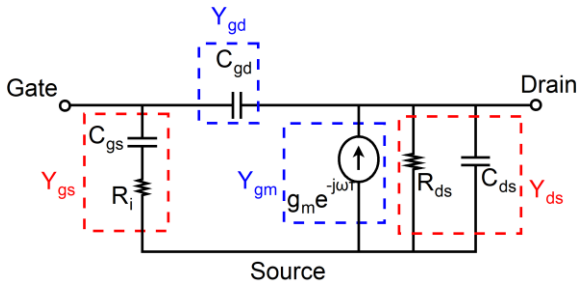

Fig. 3. The equivalent circuit of the intrinsic device

Using the approximation that $\omega^2 C_{gs}^2 R_i^2 \approx 0$ for low frequencies, following [16], g_m and τ can be obtained from the relationships:

$$\left(\frac{1}{g_m}\right)^2 \omega^2 = \frac{1}{C_{gs}^2}\left|\frac{Y_{gs}}{Y_{gm}}\right|^2 \quad (14)$$

$$\omega\tau = -phase\left(j\omega C_{gs}\left(\frac{Y_{gm}}{Y_{gs}}\right)\right) \quad (15)$$

The extraction process of C_{gs}, C_{ds}, C_{gd}, g_{ds}, R_i, g_m, and τ can be obtained from (9)-(15) using curve fitting. For example, based on (9), C_{gd} can be obtained as the slope of the line fitting $-Im\left(Y_{12}^i\right)$ with ω.

2) Analytical expression based methods

Rather than extracting the intrinsic component by data-fitting followed by optimization, analytical expressions for the intrinsic component values that minimize the L_2 norm of the error between the equivalent model and the measurement can be used [17][28][29]. These analytical approaches offer improved computational efficiency over optimization-based approaches. The analytical expressions are given as[17][28]:

$$R_i = \frac{\sum_k Re\left(Y_{gs}(f_k)\right)}{\sum_k |Y_{gs}(f_k)|^2} \quad (16)$$

$$C_{gs} = \frac{\frac{1}{2\pi}\sum_k\left(|Y_{gs}(f_k)|/f_k\right)^2}{\sum_k Im\left(Y_{gs}(f_k)\right)/f_k} \quad (17)$$

$$G_{ds} = \frac{\sum_k Re(Y_{ds}(f_k))/f_k}{\sum_k 1/f_k} \quad (18)$$

$$C_{ds} = \frac{1}{2\pi}\frac{\sum_k Im(Y_{ds}(f_k))}{\sum_k f_k} \quad (19)$$

$$C_{gd} = \frac{1}{2\pi}\frac{\sum_k\left(|Y_{gd}(f_k)|/f_k\right)^2}{\sum_k Im\left(Y_{gd}(f_k)\right)/f_k} \quad (20)$$

$$G_m = \frac{\sum_k |Y_{gm}(f_k)\left(1 + j2\pi f_k C_{gs} R_i\right)|/f_k}{\sum_k \frac{1}{f_k}} \quad (21)$$

Here, the sums are simply carried out over all k supporting frequency points (f_k). However, these expressions are derived for a transistor operating in a bias range where it acts largely as a voltage-controlled current source. Hence for the extraction at bias points for which the device is off ($V_{gs} < V_{th}$), an alternative approach (e.g. data fitting as in section B section 1) is needed [18].

C. Intrinsic current generator modelling

Accurate modelling of the current generator, especially the knee region, is critical to enable accurate design of high efficiency amplifiers. Several models of the I-V characteristics of HEMTs [30], are variants of the initial model of the I-V proposed by Angelov [9][10], as given by

$$I_{ds} = I_{pk} \underbrace{(1+\tanh(\Psi))}_{P1} \underbrace{(1+\lambda V_{ds})}_{P2} \underbrace{\tanh(\alpha V_{ds})}_{P3} \quad (22)$$

where, Ψ is a function of gate (V_{gs}) and drain (V_{ds}) voltages and α is a function of V_{gs}. The first term (P1) of (22) gives the dependence of the drain current on the gate voltage, the second term (P2) describes the saturation velocity, and the third term (P3) describes the widening of the channel and soft breakdown due to drain voltage influence. The I-V model in (22) requires the extraction of 20 parameters from the measured I-V. Additional parameters are required to model the trapping and thermal effects.

D. Fine tuning the model

The extracted values of the components require further optimization/tuning to improve the accuracy of the model. We utilize the eight-step procedure [24], shown in Table I, to optimize elements rather than optimizing all the components in a single step. This partitioning of the optimization problem into steps is based on the relative sensitivity of the S-parameters to the variation of elements. In each step, a selected combination of components, shown in Table I, is varied to find a least-squares fit of an S-parameter of the equivalent model with that of the measurement. For example, the output reflection coefficient of the device (S_{22}) is the most sensitive to a change in R_{ds} and C_{ds} [31] and hence, when these two elements are varied or optimized, the target is to minimize the error in S_{22}. These steps are performed in sequential order and repeated until the average relative percentage error between the S-parameters of the measurement and equivalent model (E_{rel}) is minimized. E_{rel} is calculated as

$$E_{rel} = \frac{1}{4N}\sum_{i=1}^{2}\sum_{j=1}^{2}\sum_{n=1}^{N}\frac{\left|S_{ij}^{Meas}(f_n) - S_{ij}^{M}(f_n)\right|}{\left|S_{ij}^{Meas}(f_n)\right|} \quad (23)$$

where, f_n denotes the n^{th} sampling frequency, and S^{Meas} and S^{M} denote the measured and modelled S-parameters, respectively.

III. Extraction Example

To illustrate the extraction of parasitics, we present two examples:

1. Equivalent model extracted from the vendor model for a Cree CGH40010F device. This illustrates the modelling up to 6 GHz covering the sub- 6 GHz 5G frequencies.

The extracted parasitic elements before and after optimization are summarized in Table II. Rather than using the function-based I-V model as in (22), we model the current generator as a table-based-model for this case. The percentage change of R_s and L_s due to the step of optimisation is the highest because of the shortfall of the extraction process [14]. The large percentage change in τ and R_i can be attributed to error propagation as their accuracy depends on the accuracy of C_{gs} [18]. E_{rel} before and after optimization are 8% and 5.9% respectively over the frequency range 0.5 GHz to 6 GHz. The S-parameters of the extracted equivalent model after optimization and the vendor model over the frequency range 0.5 GHz to 6 GHz, plotted in Fig. 4, are in close agreement. The extracted non-linear C_{gs}, C_{gd}, and C_{ds} as a function of bias are plotted in Fig. 5. In addition, the values at a typical quiescent point (V_{dsq}=28 V and I_{dsq}=150 mA) are also provided for reference. It is worth noting that in the vendor-supplied model, C_{ds} is linear [32]. However, the C_{ds} extracted here exhibits non-linear dependence with voltage in the knee region. This illustrates that the accuracy of the extraction of C_{ds} deteriorates in the knee region. Based on Fig. 5, we have modelled C_{gd} and C_{gs} as

TABLE I: Eight steps in the iterative routine used from optimizing the component values

Step	Elements optimized	S-parameter fitted	Frequency range
1	R_{ds}, C_{ds}	S_{22}	All
2	C_{gs}	S_{11}	all
3	C_{gd}, R_s	S_{12}	all
4	g_m	S_{21}	all
5	R_d, L_d, C_{pd}	S_{22}	upper half
6	R_g, L_g, C_{pg}, R_i	S_{11}	upper half
7	L_s	S_{12}	upper half
8	τ	S_{21}	upper half

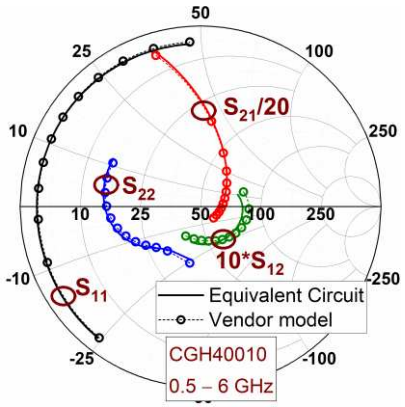

Fig. 4. Comparison of the S-parameters of the equivalent model after optimization with the S-parameters of vendor model of CGH40010 at V_{dsq}=28 V and I_{dsq}=150 mA.

TABLE II: The extracted parasitic components of the equivalent model from the vendor model of CGH40010 at I_{DSQ}=150 mA and V_{DSQ}=28 V

	Before Optimization	After Optimization	% Change
C_{pg} (in pF)	0.46	0.404	-12.2
C_{pd} (in pF)	0.46	0.404	-12.2
L_s (in nH)	0.002	0.004	100
L_d (in nH)	0.812	0.79	-2.7
L_g (in nH)	0.794	0.798	0.5
R_s (in Ω)	0.06	0.04	-33.3
R_d (in Ω)	1.486	1.28	-13.9
R_g (in Ω)	0.793	0.616	-22.3
C_{gs} (in pF)	6.982	7.332	5
C_{ds} (in pF)	0.896	1.1	22.8
C_{gd} (in pF)	0.234	0.215	-8.1
R_{ds} (in Ω)	126.582	113.73	-10.2
G_m (in S)	0.565	0.581	2.9
R_i (in Ω)	0.64	0.37	-42.2
Tau (in ps)	1.845	2.003	8.6

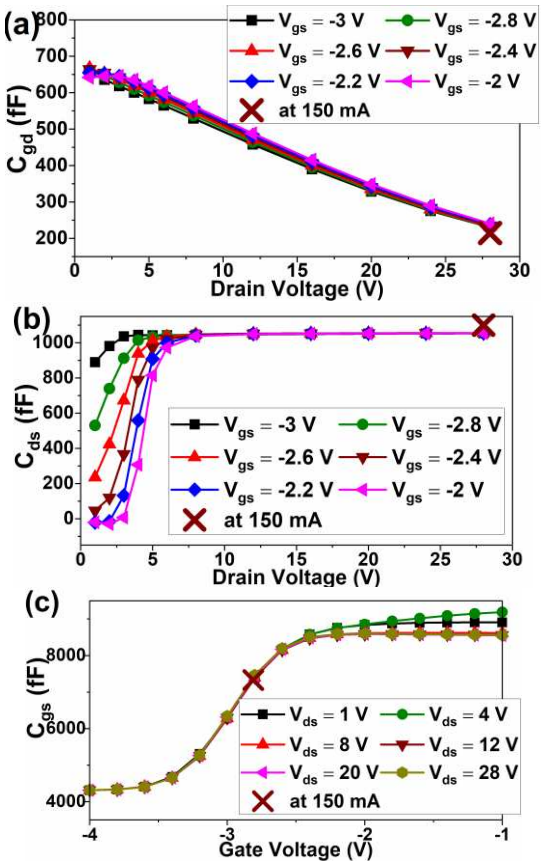

Fig. 5. Extracted values of (a) C_{gd} (b) C_{ds} (c) C_{gs} from the vendor model for V_{gs} between -2 V and -3 V and V_{ds} between 0 V and 28 V [18].

proportional to an exponential function of the drain voltage and hyperbolic tangent function of the gate voltage respectively. For implementation, these nonlinear capacitors are implemented as a charge-based model (obtained by integrating capacitance) in ADS.

2. The equivalent model is extracted from the S-parameters of a 50 nm x 75 µm GaN HEMT modelled and simulated in Synopsys Sentaurus TCAD up to 80 GHz, enabling coverage of the 5G spectrum near 30 GHz. For this case, we find that extracted extrinsic elements are negative, hence we fit the intrinsic device to the simulated data.

The extracted intrinsic elements before and after optimization for this device are summarized in Table III. Similar to the case of CGH40010, a table-based-model is used for the current generator, and the optimization process is found to change τ and R_i more than the intrinsic capacitances. The S-parameters of the extracted equivalent model after optimization and the TCAD simulation over the frequency range 0.1 GHz to

TABLE III: THE EXTRACTED PARASITIC COMPONENTS OF THE EQUIVALENT MODEL FROM THE S-PARAMETERS OF TCAD SIMULATION OF A 50 NM X 75 UM GAN HEMT AT VDSQ=5 V AND VGSQ=-2.3 V

	Before Optimization	After Optimization	% Change
τ	1.360761013	0.3	77.953513
C_{gs}	25.78278022	25.78278022	0
C_{gd}	8.112709351	8.32	2.55513467
R_i	3.81997636	3	21.4654826
C_{ds}	6.029898267	5.2	13.7630559

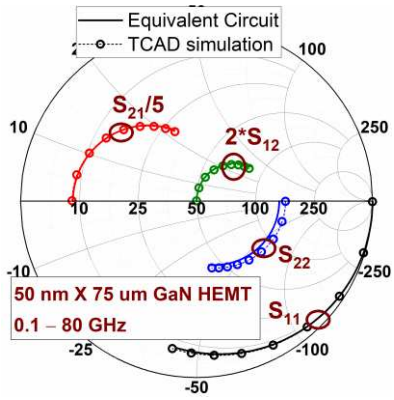

Fig. 6. Comparison of the S-parameters of the equivalent model after optimization with the S-parameters from the TCAD simulation of a 50 nm X 75 µm GaN HEMT at V_{dsq}=5 V and V_{gsq}=-2.3 V.

80 GHz, compared in Fig. 6, show a close match. The extracted nonlinear C_{gd}, C_{ds}, C_{gs}, and g_m are plotted in Fig. 7. The extracted

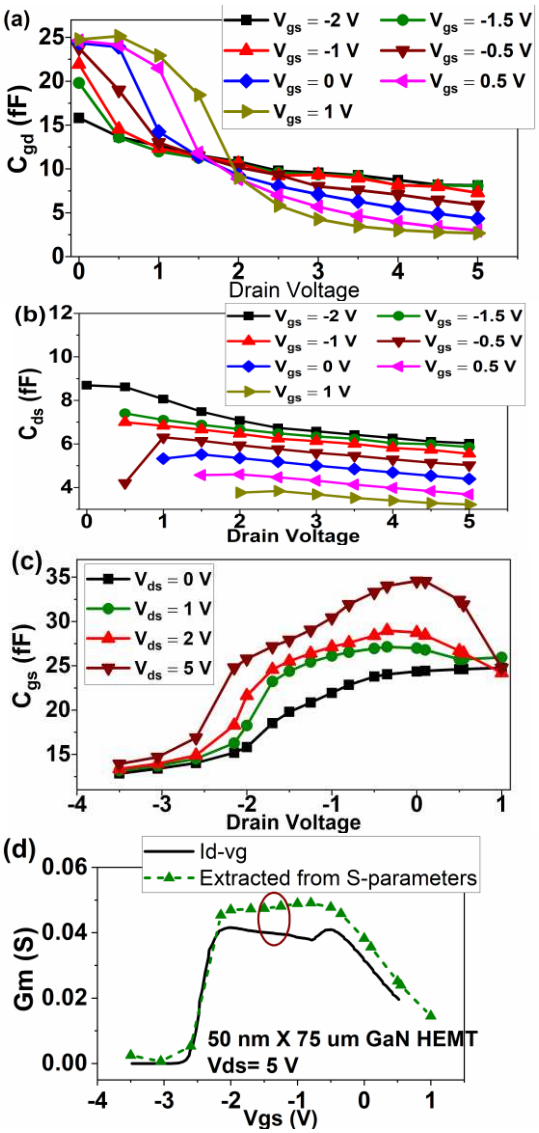

Fig. 7. Extracted values of (a) C_{gd} (b) C_{ds} (c) C_{gs} (d)g_m from the simulated S-parameters of a 50 nm X 75 um GaN HEMT device model in Synopsys Sentaurus TCAD.

g_m from S-parameters compared with IVs shows a slight discrepancy. Hence, the I-V is slightly scaled to get a good match in Fig. 6. Although the use of a table-based-model for the current generator minimizes the effort required to model the device, incorporating the effect the trapping is difficult in this approach. However, low frequency dispersion can be modelled using an additional RF source [9]. Additionally, the variation of transconductance and output conductance with frequency incorporated in this RF current source, could address the discrepancy observed in Fig. 7 (d).

IV. CONCLUSIONS

The challenges and considerations for modelling the extrinsic parasitics in a high frequency device model are presented. A modified version of the extraction procedure for extrinsic parasitics by Dambrine, Flores, and Lin is implemented for frequencies less than 6 GHz. Our method for the extraction of intrinsic parasitics is extended up to 80 GHz. Owing to its simplicity the applicability to high frequencies eases modelling effort.

REFERENCES

[1] H. Wang *et al.*, "Power Amplifiers Performance Survey 2000-Present," 2021. [Online]. Available: https://gems.ece.gatech.edu/PA_survey.html.

[2] S. C. Cripps, P. J. Tasker, A. L. Clarke, J. Lees, and J. Benedikt, "On the continuity of high efficiency modes in linear RF power amplifiers," *IEEE Microw. Wirel. Components Lett.*, vol. 19, no. 10, pp. 665–667, 2009.

[3] J. H. Kim, S. J. Lee, B. H. Park, S. H. Jang, J. H. Jung, and C. S. Park, "Analysis of High-Efficiency Power Amplifier Using Second Harmonic Manipulation : Inverse Class-F / J Amplifiers," *IEEE Trans. Microw. Theory Tech.*, vol. 59, no. 8, pp. 2024–2036, 2011.

[4] V. Carrubba *et al.*, "The continuous inverse class-F mode with resistive second-harmonic impedance," *IEEE Trans. Microw. Theory Tech.*, vol. 60, no. 6 PART 2, pp. 1928–1936, 2012.

[5] N. Poluri and M. M. De Souza, "High-Efficiency Modes Contiguous With Class B/J and Continuous Class F^{-1} Amplifiers," *IEEE Microw. Wirel. Components Lett.*, vol. 29, no. 2, pp. 137–139, Feb. 2019.

[6] F. Heinz, D. Schwantuschke, A. Leuther, and O. Ambacher, "Highly Scalable Distributed High Electron Mobility Transistor Model," in *Asia-Pacific Microwave Conference (APMC)*, 2019, pp. 1490–1492.

[7] Q. Chen, "Latest advances in gallium nitride HEMT modeling," in *2014 12th IEEE International Conference on Solid-State and Integrated Circuit Technology (ICSICT)*, 2014, pp. 1–4.

[8] Verspecht and D. E. Root, "Polyharmonic distortion modeling," *IEEE Microw. Mag.*, vol. 7, no. 3, pp. 44–57, Jun. 2006.

[9] I. Angelov, N. Rorsman, J. Stenarson, M. Garcia, and H. Zirath, "An empirical table-based FET model," *IEEE Trans. Microw. Theory Tech.*, vol. 47, no. 12, pp. 2350–2357, 1999.

[10] I. Angelov, H. Zirath, and N. Rosman, "A new empirical nonlinear model for HEMT and MESFET devices," *IEEE Trans. Microw. Theory Tech.*, vol. 40, no. 12, pp. 2258–2266, 1992.

[11] I. Angelov *et al.*, "Large-signal modelling and comparison of AlGaN/GaN HEMTs and SiC MESFETs," in *2006 Asia-Pacific Microwave Conference*, 2006, pp. 279–282.

[12] L. Dunleavy, C. Baylis, W. Curtice, and R. Connick, "Modeling GaN: Powerful but Challenging," *IEEE Microw. Mag.*, vol. 11, no. 6, pp. 82–96, 2010.

[13] J. Xu, R. Jones, S. A. Harris, T. Nielsen, and D. E. Root, "Dynamic FET model - DynaFET - for GaN transistors from NVNA active source injection measurements," in *2014 IEEE MTT-S International Microwave Symposium (IMS2014)*, 2014, pp. 1–3.

[14] M. Rasheduzzaman, "Contributing Towards Improved Communications Systems for Future Cellular Networks," PhD thesis, Department of Electronic and Electrical Engineering, University of Sheffield, 2016.

[15] G. Dambrine, A. Cappy, F. Heliodore, and E. Playez, "A New Method for Determining the FET Small-Signal Equivalent Circuit," *IEEE Trans. Microw. Theory Tech.*, vol. 36, no. 7, pp. 1151–1159, 1988.

[16] J. A. Z. Flores, "Device Characterization and Modeling of Large-Size GaN HEMTs," PhD thesis, Department of Electrical Engineering and Computer Science, University of Kassel, Germany, 2012.

[17] F. Lin and G. Kompa, "Efficient FET model parameter extraction using multi-plane data-fitting and bidirectional search technique," in *1993 IEEE MTT-S International Microwave Symposium Digest*, 1993, pp. 1021–1024.

[18] N. Poluri, "Contributing to Second Harmonic Manipulated Continuum Mode Power Amplifiers and On-Chip Flux Concentrators," PhD Thesis, The University of Sheffield, 2020.

[19] M. Berroth and R. Bosch, "High-frequency equivalent circuit of GaAs FET's for large-signal applications," *IEEE Trans. Microw. Theory Tech.*, vol. 39, no. 2, pp. 224–229, 1991.

[20] D. Lovelace, J. Costa, and N. Camilleri, "Extracting small-signal model parameters of silicon MOSFET transistors," *IEEE MTT-S Int. Microw. Symp. Dig.*, vol. 2, pp. 865–868, 1994.

[21] A. Jarndal, A. Z. Markos, and G. Kompa, "Improved Parameter Extraction Method for GaN HEMT on Si Substrate," in *IEEE International Microwave Symposium Digest*, 2010, pp. 1668–1671.

[22] J. Lu, Y. Wang, L. Ma, and Z. Yu, "A new small-signal modeling and extraction method in AlGaN/GaN HEMTs," *Solid. State. Electron.*, vol. 52, no. 1, pp. 115–120, 2008.

[23] A. Jarndal and G. Kompa, "A new small-signal modeling approach applied to GaN devices," *IEEE Trans. Microw. Theory Tech.*, vol. 53, no. 11, pp. 3440–3448, Nov. 2005.

[24] H. Kondoh, "An Accurate FET Modelling from Measured S-Parameters," in *IEEE MTT Symposium Dig.*, 1986, pp. 377–380.

[25] F. Schnieder, O. Bengtsson, F.-J. Schmuckle, M. Rudolph, and W. Heinrich, "Simulation of RF Power Distribution in a Packaged GaN Power Transistor Using an Electro-Thermal Large-Signal Description," *IEEE Trans. Microw. Theory Tech.*, vol. 61, no. 7, pp. 2603–2609, Jul. 2013.

[26] G. Crupi, A. Caddemi, D. M. M.-P. Schreurs, and G. Dambrine, "The large world of FET small-signal equivalent circuits (invited paper)," *Int. J. RF Microw. Comput. Eng.*, vol. 26, no. 9, pp. 749–762, Nov. 2016.

[27] M. Ohlrogge *et al.*, "Small signal modelling approach for submillimeter wave III-V HEMTs with analysation and optimization possibilities," in *IEEE MTT-S International Microwave Symposium Digest*, 2016, vol. 2016-Augus.

[28] F. Lin and G. Kompa, "FET model parameter extraction based on optimization with multiplane data-fitting and bidirectional search-a new concept," *IEEE Trans. Microw. Theory Tech.*, vol. 42, no. 7, pp. 1114–1121, 1994.

[29] B. L. Ooi, Z. Zhong, and M. S. Leong, "Analytical extraction of extrinsic and intrinsic FET parameters," *IEEE Trans. Microw. Theory Tech.*, vol. 57, no. 2, pp. 254–261, 2009.

[30] Y. Tao, Z. F. Hu, and Y. Fan, "A HEMT large-signal model for use in the design of microwave switching circuits," *Int. J. RF Microw. Comput. Eng.*, vol. 30, no. 3, Mar. 2020.

[31] J. W. Bandler and Q. J. Zhang, "An Automatic Decomposition Technique for Device Modelling and Large Circuit Design," in *MTT-S International Microwave Symposium Digest*, 1987, pp. 709–712.

[32] R. S. Pengelly, S. M. Wood, J. W. Milligan, S. T. Sheppard, and W. L. Pribble, "A review of GaN on SiC high electron-mobility power transistors and MMICs," *IEEE Trans. Microw. Theory Tech.*, vol. 60, no. 6 PART 2, pp. 1764–1783, 2012.